HHS Public Access

Author manuscript

Ann Neurol. Author manuscript; available in PMC 2016 April 22.

Published in final edited form as:

Ann Neurol. 2002 January ; 51(1): 102–112.

Novel Delta Subunit Mutation in Slow-Channel Syndrome Causes Severe Weakness by Novel Mechanisms

Christopher M. Gomez, MD, PhD[1], **Ricardo A. Maselli, MD**[2], **Bhupinder P. S. Vohra, PhD**[1], **Manuel Navedo, MS**[3], **Joel R. Stiles, MD, PhD**[4,5], **Pierre Charnet, PhD**[6], **Kelly Schott, BS**[1], **Legier Rojas, PhD**[3], **John Keesey, MD**[7], **Anthony Verity, MD**[8], **Robert W. Wollmann, MD, PhD**[9], and **Jose Lasalde-Dominicci, PhD**[3]

[1]Departments of Neurology and Neuroscience, University of Minnesota, Minneapolis, MN [2]Section of Neuroscience, University of California at Davis, Davis, CA [3]Department of Biology, University of Puerto Rico, San Juan, Puerto Rico [4]Biomedical Applications Group, Pittsburgh Supercomputing Center, Carnegie Mellon University and [5]Department of Neuroscience, University of Pittsburgh, Pittsburgh, PA [6]CRBM, CNRS UPR 1086, Montpellier Cedex, France [7]Departments of Neurology and Neuropathology, UCLA Medical Center, Los Angeles, CA [8]Departments of Neuropathology, UCLA Medical Center, Los Angeles, CA [9]Departments of Pathology and Neurology, University of Chicago, Chicago, IL

Abstract

We investigated the basis for a novel form of the slow-channel congenital myasthenic syndrome presenting in infancy in a single individual as progressive weakness and impaired neuromuscular transmission without overt degeneration of the motor endplate. Prolonged low-amplitude synaptic currents in biopsied anconeus muscle at 9 years of age suggested a kinetic disorder of the muscle acetylcholine receptor. Ultrastructural studies at 16 months, at 9 years, and at 15 years of age showed none of the typical degenerative changes of the endplate associated with the slow-channel congenital myasthenic syndrome, and acetylcholine receptor numbers were not significantly reduced. We identified a novel C-to-T substitution in exon 8 of the δ-subunit that results in a serine to phenylalanine mutation in the region encoding the second transmembrane domain that lines the ion channel. Using *Xenopus* oocyte in vitro expression studies we confirmed that the δS268F mutation, as with other slow-channel congenital myasthenic syndrome mutations, causes delayed closure of acetylcholine receptor ion channels. In addition, unlike other mutations in slow-channel congenital myasthenic syndrome, this mutation also causes delayed opening of the channel, a finding that readily explains the marked congenital weakness in the absence of endplate degeneration. Finally, we used serial morphometric analysis of electron micrographs to explore the basis for the progressive weakness and decline of amplitude of endplate currents over a period of 14 years. We demonstrated a progressive widening and accumulation of debris in the synaptic cleft, resulting in loss of efficacy of released neurotransmitter and reduced safety factor. These studies demonstrate the role of previously unrecognized mechanisms of impairment of synaptic

Address correspondence to Dr Gomez, Departments of Neurology and Neuroscience, MMC 295, University of Minnesota, 420 Delaware St. SE, Minneapolis, MN 55455.

transmission caused by a novel mutation and show the importance of serial in vitro studies to elucidate novel disease mechanisms.

In its classical form, the slow-channel congenital myasthenic syndrome (SCCMS) is characterized by progressive weakness and fatigability of the voluntary muscles as a result of impaired neuromuscular transmission. SCCMS is attributed to the consequences of missense mutations in the skeletal muscle acetylcholine receptor (AChR) that alter the gating kinetics of the AChR ion channel. The pathological hallmark of the SCCMS, the endplate myopathy, consists of degeneration of postsynaptic folds, subsynaptic nuclei, and mitochondria, as well as accumulation of vacuoles in the subsynaptic region.[1–4] Up to 12 distinct mutations have been detected in the genes encoding the α-, β-, and ε-subunit of the AChR within regions encoding the first three transmembrane domains (M1–3) or ligand-binding domain. Individual cases of SCCMS demonstrate marked differences in clinical severity, in the nature of the AChR kinetic abnormality, and in the ultrastructural changes of the neuromuscular junction (NMJ).[3–9]

It has been proposed that the weakness, muscle atrophy, and endplate myopathy seen in SCCMS are caused by the prolonged AChR channel openings through a sequence of events initiated by calcium overload and culminating in degeneration of subsynaptic organelles and the postsynaptic membrane, AChR loss, diminished endplate potentials, and reduced safety factor of neuromuscular transmission.[1,3,4] We recently identified a patient with severe SCCMS in whom end-plate potentials were markedly diminished in childhood and further deteriorated in adolescence in the absence of overt endplate myopathy. This finding suggested that distinct, unrecognized mechanisms might account for this patient's clinical and electrophysiological abnormalities. We report here molecular genetic evidence, in vitro expression studies, and serial ultrastructural studies over 14 years showing that the deficit in neuromuscular transmission in an individual with a novel δ-subunit mutation results from delayed ion channel opening and progressive remodeling and widening of the cleft of the neuromuscular junction.

Patient and Methods

Clinical Data

The patient, currently 15 years of age, was the product of a non-consanguineous marriage and was born after an uncomplicated 34-week pregnancy and delivery. At 1 month of age, he appeared floppy, with poor head control. At 6 months, eyelid ptosis was observed, and at 10 months, he was still unable to sit without support. Serum creatine kinase and edrophonium tests were normal. At 16 months, he began to walk but required rest every 2 to 4 m. Intercostal muscle biopsy was performed at age 16 months (biopsy 1). At age 9 years, the patient required a wheelchair and support when sitting and developed difficulty chewing and swallowing. Anticholinesterase medications produced no improvement. A left anconeus muscle biopsy was performed at this time (biopsy 2). The weakness continued to progress with two episodes of respiratory failure at age 14, one requiring ventilatory assistance. At age 15, a right anconeus muscle biopsy was performed (biopsy 3). Neurological examination showed normal mental development and sensation, normal muscle bulk, but severe

weakness, and fatigability in all muscles. There was no history of neuromuscular disease in either parent or in two half-siblings.

Venous blood samples from the patient, his parents, and two half-siblings and muscle biopsies were obtained under procedures approved by the institutional human studies review boards. Normal human genomic DNA samples from the Centre d'Etude du Polymorphisme Humain panel were used as control DNA.

Clinical Electrophysiological Studies

Clinical electromyographic recordings were performed at ages 9 years and 15 years. In both studies, nerve conduction velocity studies and repetitive stimulation of the right median and ulnar nerves were performed using conventional techniques of skin surface nerve stimulation and recording. In vitro microelectrode studies were performed on the left anconeus muscle at age 9 and the right anconeus muscle age 15 as previously described.[10,11]

Genetic Analysis of AChR Subunit Genes

Polymerase chain reaction and single-strand conformation polymorphism (SSCP) analyses used to amplify and screen the second transmembrane (M2) domains of the four adult AChR subunits were performed as described,[5] except that nucleotide sequence analysis of DNA templates amplified from genomic DNA or from SSCP conformers was performed on an automated DNA sequencer (ABI 377, Applied Biosystems, Foster City, CA). To exclude the presence of additional mutations, the nucleotide sequence of the remainder of the coding regions for the four AChR subunits was determined for exon segments amplified from the patient genomic DNA (primer sequences available upon request).

In Vitro Expression Studies

Site-Directed Mutagenesis—Generation of the homologous δS268F mutation in mouse δ-subunit cDNA, preparation and injection of AChR subunit mRNA were carried out as described.[3] *Xenopus* oocytes were injected with 40 nl of mRNA (0.2 μg/μl) mixed in the ratio of 2:1:1:1 (α:β:δ:ε). Electrophysiological recording was performed 3 days after mRNA injection.

Patch-Clamp Electrophysiological Analysis—Oocyte vitelline membranes were removed manually after incubation in a hypertonic solution (150mM NaCl, 2mM KCl, 3% sucrose, and 5 mM Hepes, pH 7.6), and the oocytes were placed in a recording chamber containing bath solution (100mM KCl, 1mM $MgCl_2$, 10mM Hepes, pH 7.2, 20 to 22°C). Patch pipettes (8 to 12MΩ) were made of thick-walled borosilicate glass (Sutter Instruments, Novato, CA). The pipette solution contained 100mM KCl, 10mM Hepes, and 10 mM EGTA (pH 7.2) and, for single-channel studies, 4, 100, or 500μM ACh. All experiments were performed in a cell-attached patch configuration. Single-channel currents were recorded using an Axopatch 200B (Axon Instruments, Union City, CA), filtered at 5kHz (Frequency Devices, Haverhill, MA) and stored on VHS tapes using a digital data recorder (VR-10B, Instrutech, Mineola, NY). The data traces were played back into a Pentium IV-based computer through a DigiData 1200 interface (Axon Instruments) and digitized at 20μsec.

Single-channel events were detected with a half-amplitude crossing algorithm (pClamp6). Amplitude histograms were constructed from event list files created to include well-defined full openings, fitted by a Gaussian function with the appropriate number of components. Single-channel current amplitudes were plotted as a function of holding potential to obtain the current–voltage relationship.

Open and closed time duration distributions were constructed from pClamp6-generated files and for 4μM ACh were fitted using the maximum likelihood algorithm with the appropriate number of components. Records at 100 or 500μM ACh were fitted using the simplex least-squares algorithm with the appropriate number of components. Under our recording conditions, the apparent or effective opening rates (β-values) of the channel are obtained from closed times and depend on the ACh concentration (see kinetic scheme below).

We estimated effective β-values during bursts using 100 or 500μM ACh (5kHz, −100mV). Bursts arise from single channels as they periodically return from relatively long-lived desensitized states.[12] Each activation episode begins with the transition of a single receptor from the desensitized to the activatible state and then ends as the receptor returns to the desensitized state. Thus, in our burst-oriented analysis, bursts were defined as a series of openings separated by closures shorter than a critical duration (τ_{crit}, 3 to 5 times longer than the predominant closed time). We fitted closed interval durations to the sum of three to five exponentials, and the intracluster open probability (P_o) was calculated from the sum of open durations divided by the burst duration.[13,14]

To interpret the single-channel kinetics, we used a model with two open states:

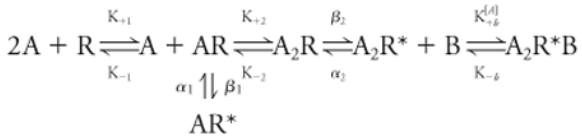

In this scheme, R is the receptor, A is ACh, A_2R is the biliganded species, AR* and A_2R* are the monoliganded and biliganded (and most abundant) open-state of the receptor–ligand complex, respectively, B is the block molecule (in this case ACh), and A_2R*B is the blocked state of the channel. k_{+1} and k_{+2} are the binding rate constants, and k_{-1} and k_{-2} the first and second dissociation rate constants for the first and second sites, respectively. α_1 and α_2 are the fast and slow closing rate constants, respectively, and β_1 and β_2 are the opening rate constants, respectively. K_{+b} is the blocking rate and k_{-b} is the rate of opening from the blocked state (later denoted β_3 in Results). We evaluated only effective channel rates associated with isomerizations to and from the two open-channel states AR* and A_2R*.

Pathological Studies

Biopsies obtained from intercostal muscle (age 16 months) and anconeus muscle (ages 9 and 15 years) were performed under procedures approved by the institutional human studies review boards. Muscle specimens were fixed in 4% glutaraldehyde and prepared for electron microscopy as described.[15]

Electron micrographs of all identifiable NMJs in three biopsies of the patient and from four other control patients were printed at 5 to 30K magnification and scanned at 600dpi using a Bio-Rad flatbed scanner. Tiff images were analyzed using the imaging program Photoshop (Adobe). To obtain an index of mean width of the synaptic cleft, the width was measured at five to six points for each NMJ. To correct for differences in print magnification, cleft width was normalized to the mean width of the Z lines (~0.1μM) in the same image.

Determination of Endplate AChR Number

The number of AChRs per endplate was estimated by determining the number of α-bungarotoxin (αBT) binding sites per cholinesterase-stained endplate.[16] Briefly, 12 to 20 fine muscle fiber bundles of the anconeus muscle were dissected and incubated at room temperature for 3 hours in Ham's F-12 culture medium containing 1μM ^{125}I-αBT, washed 6 times for 2 hours, and fixed overnight in freshly prepared 4% paraformaldehyde. The endplates were localized by means of a histochemical stain for cholinesterase,[17] the muscle fiber bundles were trimmed to 1- to 2mm lengths with and without endplates, and their radioactivity (counts per minute) determined in a Gamma 5500B, Beckman gamma counter. The specific counts per minute for bundles with endplates were determined by subtraction of the background counts per minute for endplate-free bundles. The ratio of the specific counts per minute for endplate bundles to the number of fibers in the bundle is equivalent to the αBT binding per endplate. From this value the number of AChRs per endplate can be calculated, assuming two binding sites per receptor. All statistical comparisons were made using a two-tailed *t* test assuming unequal variances.

Results

Electrophysiological Studies

Compound muscle action potentials (CMAP) evoked by single stimuli to either median or ulnar nerves were followed by prominent repetitive discharges (Fig 1A). Repetitive stimulation of the ulnar nerve at 2Hz elicited a profound decremental response in the CMAP amplitude, recorded at 44% in the second study (Fig 1B).

In microelectrode studies of biopsied anconeus muscles, there was a severe reduction of miniature endplate potential (MEPP) amplitudes (43%) in the study performed at the age of 9 years. This reduction became even more profound (73%) in the study performed at 15 years (Table 1; see Fig 1). In addition, in the second study, the quantal content of endplate potentials (EPPs) was reduced by 57% in comparison with control muscles. Voltage-clamp studies showed that MEPC amplitudes were reduced by 61% in the first study and were unobtainable in the study performed at age 15 years. Exponential fitting of MEPC and EPC decay phases demonstrated greater than sixfold prolongation, but because of the small size of the MEPCs, a biphasic component could not be resolved. Finally, nerve stimulation at physiological rates of muscle activation (20 to 30Hz) showed the typical “staircase phenomenon” of summation of prolonged EPPs, providing evidence of activation-dependent endplate depolarization.[18]

These results indicate a severe reduction in safety factor of neuromuscular transmission that was responsible for the clinical findings of weakness and fatiguability. Moreover, our findings indicate that impairment in safety factor worsened with time, concomitant with the clinical deterioration. The abnormal EPC decay phase suggested a kinetic abnormality in the AChR channel caused by an AChR subunit mutation.

Molecular Genetic Studies

Based on the electrophysiological findings, we investigated the possibility of a mutation in one of the genes encoding the four AChR subunits. SSCP screening the M2 domains of the four adult AChR subunits of the proband showed two distinct conformers in the DNA amplified from δ-subunit exon 8, which encodes the δ-subunit M2 domain (Fig 2A, lane 4, arrow). Only a single conformer was present in DNA amplified from the δ-subunit M2 region of the genomic DNA of the parents and siblings and of 100 normal controls (see Fig 2A, lanes 1–3).

Direct sequencing of SSCP conformers demonstrated that the abnormal SSCP conformer contained a C-to-T transition within codon 268, coding for a serine-to-phenylalanine substitution (S268F) in the twelfth residue of the δ-subunit M2 domain (see Fig 2B, mutant allele, arrow). This mutation was not present in the sequence amplified from the normal conformer (see Fig 2B, normal allele). The δ-subunit M2 DNA amplified from the patient's genomic DNA contained both the wild-type and mutant sequences (see Fig 2B, patient), while the δ-subunit M2 regions amplified from genomic DNA of both parents (Fig 2B, mother) contained only the normal sequence. Direct nucleotide sequence analysis failed to show any additional mutations in the coding regions for the α-, β-, δ-, and e-subunits of this patient (not shown).

Figure 3 shows aligned sequences of δ-subunit M2 domains from six species, and the M2 domains of six other human AChR subunits. The codon 268 residue is completely conserved among the δ-subunits shown and is highly conserved among M2 domains of other nicotinic AChR subunits.

In Vitro Expression Studies

To investigate the effect of the novel δ-subunit mutation on AChR channel function and explain the basis for the weakness and impaired neuromuscular transmission, we studied the properties of the homologous mutation δS268F in mouse AChRs expressed in *Xenopus* oocytes. The slope of the current–voltage relationship for δS268F–AChRs is essentially identical to that of wild type AChRs and corresponds to a single channel conductance of 60 pS (Fig 4A). Thus, diminished MEPC amplitudes cannot be explained by an effect of the δS268F mutation on channel conductance.

To determine the effect of the δS268F mutation on mean open duration, we recorded single-channel currents at low ACh concentration (4μM, where interruptions of open time by channel block are infrequent). As shown in Figure 4B and Table 2, the intraburst open probability increased, with an apparent increase in open time for biliganded AChRs of more than sevenfold. This change is consistent with the observed prolongation of MEPC decay times (see Fig 1C and Table 1).

To analyze further the kinetics of activation of the mutant δS268F-AChRs, single-channel currents were elicited at high ACh concentrations (100μM or 500μm ACh, Table 3; see Fig 4C). As ACh concentration increases, the fraction of biliganded AChRs also increases, and thus the recordings provide an increasingly sensitive estimate of apparent opening rate and channel block. As summarized for the mutant channel in Figure 4C and Table 3, (1) short intraburst closures can be incomplete (best seen in Fig 4C at 100μm ACh); (2) the apparent closing rate increases more rapidly than for the wild-type as ACh concentration increases, suggesting an increased propensity for open channel block; and (3) the apparent opening rate is decreased (β_1, β_2, and β_3 values at 500μm ACh) by 1.5-to 3.4-fold. All these observations suggest markedly increased steric hindrance in the channel, introduced by the large mutant phenylalanine residue in place of the wild-type serine.

Toxin-Binding and Pathological Studies

Impaired neuromuscular transmission and weakness in classical SCCMS is attributed to reduced AChR num-bers at the endplate.[1] We estimated the number of AChRs present in the NMJ in biopsy 3 by determining the specific αBT binding as a fraction of histochemically identified motor endplates in each muscle fiber. The AChR number per endplate in the patient ($1.53 \pm 0.41 \times 10^7$ n = 10) was not significantly different from the AChRs/endplate in controls ($1.83 \pm 0.71 \times 10^7$ n = 10). This finding further emphasizes the importance of the kinetic changes revealed by the expression studies in directly affecting synaptic responses.

Although in vitro expression studies provide an explanation for the change in AChR channel kinetics and for the impaired neuromuscular transmission, they could not explain the progressive deterioration in both strength and MEPP amplitude. Therefore, we performed serial pathological studies to investigate the basis for worsening synaptic function. Ultrastructural studies displayed only minimal changes in the neuromuscular junction in biopsy 1 at age 16 months. Both normal and mildly abnormal (14/22) neuromuscular junctions were identified (Fig 5A). Abnormal endplates had slightly widened synaptic cleft or had regions of postsynaptic membrane in which no nerve terminus was visible. This observation suggested the occurrence of remodeling or reinnervation.[19] In biopsy 2 (age 9) (see Fig 5B), nearly all NMJs appeared abnormal (8/10). The width of the synaptic cleft was more variable and numerous endplate regions were innervated by two nerve termini. The postsynaptic membrane frequently extended far beyond the proximity of the nerve terminus. Small collections of amorphous debris were found in some of the clefts. In biopsy 3 (age 15), the changes in the cleft were dramatic, and all neuromuscular junctions (9/9) were abnormal (see Fig 5C). Nerve terminals frequently appeared shrunken and widely separated from the postsynaptic membrane. The primary clefts were filled with amorphous or globular debris. There were numerous areas of postsynaptic membrane that were not associated with a nerve terminal. In rare cases, degenerating folds could be seen.

The mean cleft width of the NMJ profiles of the three patient biopsies and four control biopsies were compared by normalizing to the width of the Z line of the sarcomeres in each field (Fig 6). The control value of 57 to 69nm agrees well with previous estimates of cleft width.[20] The width of the primary cleft was increased in all three patient biopsies (see Fig 6). More importantly, the width of the primary cleft underwent a dramatic increase by the

third biopsy, suggesting a morphological and structural basis for progressive weakness and reduction in MEPP amplitude.

Discussion

We describe the molecular and physiological basis for a unique form of SCCMS attributed to a novel mutation in the δ-subunit of the AChR. In this patient pronounced weakness in infancy and progressive weakness in adolescence could not be explained by the presence of a classical endplate myopathy. We found that the patient, but neither parent, bore a mutation in the AChR δ-subunit, predicting a serine to phenylalanine substitution at position 268 in the ion-channel domain, M2. As with other SCCMS mutations, the δS268F mutation causes delayed channel closing when expressed in mouse AChRs in vitro. In addition, this mutation tended to prevent complete channel closure, increased the propensity for open-channel block, and, most importantly, reduced the rate of channel opening. Because the opening rate determines the probability that AChRs open in response to released ACh this change can have a significant effect on the amplitude of the synaptic currents. Finally, using serial biopsies performed over 14 years, we demonstrated that continued progression of disease was associated with progressive reduction in MEPP amplitudes and with progressive widening of the synaptic cleft.

This case is important for several reasons: (1) it is the first report, to our knowledge, that a δ-subunit AChR mutation can result in form of SCCMS; (2) it illustrates that certain forms of SCCMS, caused by AChR mutations, can occur in the absence of endplate myopathy; (3) it demonstrates that reduced safety factor of neuromuscular transmission and diminished MEPC and EPC amplitudes may be caused by changes in AChR properties, such as the rate of AChR channel opening; and (4) it demonstrates the role of progressive synaptic remodeling in disease progression.

AChR point mutations responsible for the SCCMS have been found in transmembrane domains of the α-, β-, and ε-subunits, and in the ACh-binding domain of the α subunit in different cases or families of SCCMS.[3–9] Although this case demonstrates similar clinical and electrophysiological features, the previously studied cases had ultrastructural evidence of severe endplate myopathy and reduced AChR numbers, believed to underlie the defective neuromuscular transmission.[1,3–6,8] In the present patient, there were occasional subsynaptic vacuoles in the intercostal muscle endplates at 16 months, but in these endplates and in those of anconeus muscle at age 9 and 15 years, there was initially mild, and only later severe, widening of the cleft, with little or no degeneration of subsynaptic organelles or postsynaptic folds. Despite nearly normal AChR numbers and the absence of endplate degeneration, quantal amplitudes were reduced by approximately twofold (early, minimal cleft widening) or approximately fourfold (late, severe cleft widening).

The pathogenesis of weakness in this patient includes both established and novel mechanisms. First, the number of endplate AChRs may have been slightly reduced (16%) at age 15 years, but this change was not statistically significant. A small reduction in AChR number, or, AChR density in the postsynaptic membrane, may contribute to the reduced safety factor of neuromuscular transmission.[21] Second, a reduction in quantal content further

diminishes the safety factor by reducing the amplitude of the endplate potentials. Third, the markedly prolonged decays of MEPCs and EPCs in this patient predict staircase summation of EPP potentials leading to an activation-dependent depolarization blockade similar to that demonstrated with cholinesterase inhibitors.[18,22] Although this effect does not reduce the safety factor, it impairs the generation of muscle fiber action potentials and reduces fiber contraction.

Beyond these familiar mechanisms, the kinetic analysis and serial ultrastructural studies demonstrated at least two additional sources of weakness in this patient.

1. *Impaired neuromuscular transmission through slowed AChR channel opening:* Single-channel recordings of δS268F AChRs expressed in *Xenopus* oocytes showed a 1.5- to 3.4-fold decrease in effective opening rate. Without exhaustive and technically demanding recordings performed with extremely high bandwidth and rapid ACh application at multiple concentrations, it is very difficult to correlate apparent opening rates with actual (concentration-independent) rate constants, and the fastest rates (e.g., β_2 for wild-type AChRs) are most markedly underestimated. After taking this technical limitation into account, our data strongly suggest an overall two- to threefold decrease in actual opening rate of the mutant AChRs. Such a decrease is expected to cause significant weakness by reducing quantal and multiquantal EPC amplitudes and the safety factor of neuromuscular transmission. From modeling studies, an actual reduction in β values on the order of threefold could easily reduce the current amplitude by about twofold, because the probability that each liganded AChR opens (to initiate a burst of openings) is reduced.[23,24] In addition, the probability of reopenings within a burst would be similarly reduced, an effect that would tend to shorten the burst duration and partially offset the prolonged open time introduced by concomitant slowing of channel closure. Thus, the combined effects of a reduction in opening rate, coupled to a reduction in closing rate, would make possible an overall reduction in EPC amplitude despite an apparent increased AChR open probability within a burst.

   Although other mutations affecting the δ-subunit have not yet been identified in SC-CMS, a mutation of the homologous residue, εT264P, position 12′ of the ε-subunit M2 domain, was found in one case associated with a severe endplate myopathy.[25] Channel kinetics have been investigated after substitutions at this position in the four subunits of mouse AChR expressed in HEK cells, using choline as agonist in patch-clamp studies.[26] Not unexpectedly, most substitutions resulted in a decreased closing rate. In addition, most substitutions also increased rather than decreased the rate of channel opening. Such findings are not necessarily incompatible with our results, however, because of the difference in ligand and substituted amino acid residue (phenylalanine was not tested). Regardless, in the earlier study, the δ-subunit was more sensitive to mutations at this position than were the other three subunits.[26] This finding suggests an asymmetrical structure to the ion channel and the prominent role of residues at this position in channel opening. Therefore, it may be that the increase in volume and reduced polarity of

the phenylalanine side-chain in the δS268F mutation might cause a more dramatic steric stress to the channel-gating mechanism than do other substitutions.

A large decrease in β has not been suggested in kinetic studies of other spontaneous mutations in SCCMS.[4,7,8,27] One mutation, αN217K, identified in a patient demonstrating a typical endplate myopathy, may have caused a slight reduction in the β parameter,[27] which may have compounded the weakness resulting from the endplate myopathy. In the present case, the simplest explanation for early onset weakness in the absence of overt endplate myopathy is a relatively large reduction in opening rate.

2. *2. Deterioration in neuromuscular transmission due to widening synaptic cleft:* Weakness and impaired neuromuscular transmission in this patient clearly progressed with age. Although AChR numbers were not followed serially, they were not significantly reduced in the third biopsy at 15 years of age. However, the striking alteration was the structure of the synaptic cleft, which changed markedly over time. At both 16 months and 9 years of age, the cleft width showed marked focal increases and an average increase of up to 50%. By 15 years of age, the synaptic clefts were on average more than four times wider than normal and filled with basement membrane-like debris. The basis for the widened, debris-filled cleft may relate to the effect of chronic remodeling of areas of the neuromuscular junction, with reinnervation at sites of accumulated basement membrane debris in areas previously affected by the disease process. A widened synaptic cleft increases the distance between ACh release sites and the postsynaptic membrane, thus increasing the cleft volume into which ACh is diluted as it diffuses toward AChRs and acetylcholinesterase. Such dilution decreases the efficiency of MEPC and EPC generation, because far fewer AChRs ever become biliganded. Therefore, far fewer AChRs have an effective chance to open. Hence, the MEPC and EPC amplitude is severely reduced, which decreases the safety factor for neuromuscular transmission and contributes to the overall neuromuscular weakness.[23,28–30]

This study further demonstrates the importance of detailed evaluation of the genetic, physiological and ultrastructural basis for impaired synaptic transmission as in the SCCMS. These findings clearly justify the value of such detailed and serial evaluations, which have led to identification of two previously unrecognized (potentially novel) mechanisms of synaptic failure.

Acknowledgments

This work was supported by grants RO1 NS33202 (to CG, RAM, JLD) and NIH RR 06009 (to JRS) from the National Institutes of Health.

References

1. Engel AG, Lambert EH, Mulder DM, et al. A newly recognized congenital myasthenic syndrome attributed to a prolonged open time of the acetylcholine-induced ion channel. Ann Neurol. 1982; 11:553–569. [PubMed: 6287911]
2. Engel, AG. Myasthenic syndromes. In: Engel, AG.; Franzini-Armstrong, C., editors. Myology. 2nd. New York: McGraw-Hill; 1994. p. 393-418.

3. Gomez CM, Maselli R, et al. A β subunit mutation in the acetylcholine receptor channel gate causes severe slow-channel syndrome. Ann Neurol. 1996; 39:717–723.
4. Milone M, Wang HL, Ohno K, et al. Slow-channel myasthenic syndrome caused by enhanced activation, desensitization, and agonist binding affinity attributable to mutation in the M2 domain of the acetylcholine receptor alpha subunit. J Neurosci. 1997; 17:5651–5665. [PubMed: 9221765]
5. Gomez CM, Gammack JT. A leucine-to-phenylalanine substitution in the acetylcholine receptor ion channel in a family with the slow-channel syndrome. Neurology. 1995; 45:982–985. [PubMed: 7538206]
6. Ohno K, Hutchinson D, Milone M, et al. Congenital myasthenic syndrome caused by prolonged acetylcholine receptor channel openings due to a mutation in the M2 domain of the ε subunit. Proc Natl Acad Sci USA. 1995; 92:758–762. [PubMed: 7531341]
7. Sine SM, Ohno K, Bouzat C, et al. Mutation of the acetylcholine receptor a subunit causes a slow-channel myasthenic syndrome by enhancing agonist binding affinity. Neuron. 1995; 15:229–239. [PubMed: 7619526]
8. Engel AG, Ohno K, Milone M, et al. New mutations in acetylcholine receptor subunit genes reveal heterogeneity in the slow-channel congenital myasthenic syndrome. Hum Mol Genet. 1996; 5:1217–1227. [PubMed: 8872460]
9. Croxen R, Newland C, Beeson D, et al. Mutations in different functional domains of the human muscle acetylcholine receptor alpha subunit in patients with the slow-channel congenital myasthenic syndrome. Hum Mol Genet. 1997; 6:767–774. [PubMed: 9158151]
10. Maselli R, Nelson D, Richman D. Effects of a monoclonal anti-acetylcholine receptor antibody on the avian end-plate. J Physiol. 1989; 411:271–283. [PubMed: 2614725]
11. Maselli R, Mass D, Distad B, Richman D. Anconeus muscle: a human preparation suitable for in-vitro microelectrode studies. Muscle Nerve. 1991; 14:1189–1192. [PubMed: 1662771]
12. Sakmann B, Patlak J, Neher E. Single acetylcholine-activated channels show burst-kinetics in presence of desensitizing concentrations of agonist. Nature. 1980; 286:71–73. [PubMed: 6248795]
13. Auerbach A, Lingle CJ. Heterogeneous kinetic properties of acetylcholine receptor channels in Xenopus myocytes. J Physiol. 1986; 378:119–140. [PubMed: 2432248]
14. Auerbach A. A statistical analysis of acetylcholine receptor activation in Xenopus myocytes: stepwise versus concerted models of gating. J Physiol. 1993; 461:339–378. [PubMed: 8350269]
15. Gomez CM, Wollmann RL, Richman DP. Induction of the morphologic changes of both acute and chronic experimental myasthenia by monoclonal antibody directed against acetylcholine receptor. Acta Neuropathol (Berl). 1984; 63:131–143. [PubMed: 6610275]
16. Pestronk A, Drachman DB, Self SG. Measurement of junctional acetylcholine receptors in myasthenia gravis: clinical correlates. Muscle Nerve. 1985; 8:245–251. [PubMed: 4058469]
17. Namba T, Nakamura T, Grob D. Staining for nerve fiber and cholinesterase activity in fresh frozen sections. Am J Clin Pathol. 1967; 47:75–79.
18. Maselli RA, Leung C. Analysis of anticholinesterase-induced neuromuscular transmission failure. Muscle Nerve. 1993; 16:548–553. [PubMed: 8390609]
19. Fahim MA. Rapid neuromuscular remodeling following limb immobilization. Anat Rec. 1989; 224:102–109. [PubMed: 2729612]
20. Engel, AG. The neuromuscular junction. In: Engel, AG.; Franzini-Armstrong, C., editors. Myology. New York: McGraw-Hill; 1994. p. 261-302.
21. Lindstrom JM, Lambert EH. Content of acetylcholine receptor and antibodies bound to receptor in myasthenia gravis, experimental autoimmune myasthenia gravis, and Eaton-Lambert syndrome. Neurology. 1978; 28:130–138. [PubMed: 202890]
22. Maselli RA, Leung C. Analysis of neuromuscular transmission failure induced by anticholinesterases. Ann NY Acad Sci. 1993; 681:402–404. [PubMed: 8395155]
23. Land BR, Salpeter EE, Salpeter MM. Kinetic parameters for acetylcholine interaction in intact neuromuscular junction. Proc Natl Acad Sci USA. 1981; 78:7200–7204. [PubMed: 6947281]
24. Stiles JR, Kovyazina IV, Salpeter EE, Salpeter MM. The temperature sensitivity of miniature endplate currents is mostly governed by channel gating: evidence from optimized recordings and Monte Carlo simulations. Biophys J. 1999; 77:1177–1187. [PubMed: 10423463]

25. Ohno K, Wang HL, Milone M, et al. Congenital myasthenic syndrome caused by decreased agonist binding affinity due to a mutation in the acetylcholine receptor epsilon subunit. Neuron. 1996; 17:157–170. [PubMed: 8755487]

26. Grosman C, Auerbach A. Asymmetric and independent contribution of the second transmembrane segment 12′ residues to diliganded gating of acetylcholine receptor channels—a single-channel study with choline as the agonist. J Gen Physiol. 2000; 115:637–651. [PubMed: 10779320]

27. Wang HL, Auerbach A, Bren N, et al. Mutation in the M1 domain of the acetylcholine receptor alpha subunit decreases the rate of agonist dissociation. J Gen Physiol. 1997; 109:757–766. [PubMed: 9222901]

28. Wathey JC, Nass MM, Lester HA. Numerical reconstruction of the quantal event at nicotinic synapses. Biophys J. 1979; 27:145–164. [PubMed: 262376]

29. Salpeter, M. Vertebrate neuromuscular junctions: gerneral morphology, molecular organization, and functional consequences. In: Salpeter, M., editor. The vertebrate neuromuscular junction. New York: Alan R Liss; 1987. p. 55-115.

30. Stiles, J.; Bartol, T.; Salpeter, M., et al. Synaptic variability: new insights from reconstructions and Monte Carlo simulations with MCell. In: Cowan, W.; Stevens, C.; Sudhof, T., editors. Synapses. Baltimore: Johns Hopkins University Press; 2001. p. 681-731.

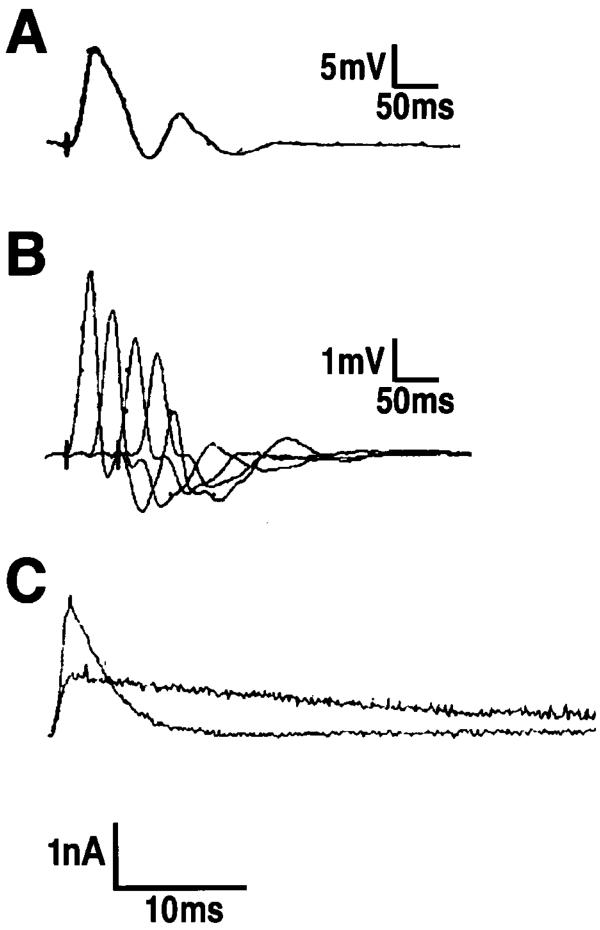

Fig 1.

Classical electrophysiological features of slow-channel congenital myasthenic syndrome. (A) Compound muscle action potentials (CMAPs) recorded over the hypothenar muscles evoked by single nerve stimulus. As is typical for SCCMS, there is a repetitive response to the single stimulus. (B) CMAPs evoked by repetitive stimulation. The amplitude of each of four successive responses decreases, indicating failure of neuromuscular transmission. (C) Superimposed miniature end-plate currents recorded from anconeus muscle of control and the proband. The prolonged waveform of the patient miniature endplate current (MEPC) has a decay time constant of 31 msec, compared with control of 3.2 msec. The MEPC amplitude of the patient is about 50% of the control. Scale bars = A: 5 mV, 50 msec; B: 1 mV, 50 msec; C: 1 nA, 10 msec.

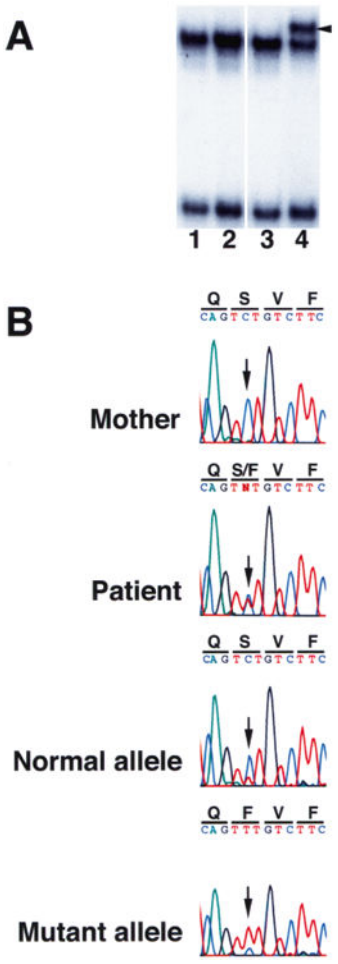

Fig 2.

(A) Single-strand conformation polymorphism gel analysis of δ-subunit exon 8 DNA fragments amplified from control *(lanes 1–3)* and patient *(lane 4)*. Shown are autoradiograms of both single strands of exon 8 DNA fragments internally labeled with ^{32}P by polymerase chain reaction-amplified using primers δ 8U4I: GTC.TGA.ATC.GAC.ACT.GGA.ACC and δ 8D: TGC.CGA.TAA.GGGGGA.TGGC. In all four lanes, the lower strand of amplified DNA does not show any difference in mobility. *Lanes 1–3*, upper strand also migrates as a single band; *lane 4*, upper strand has two distinct conformers (arrow indicates upper conformer). (B) Sequence of a portion of the plus (coding) strand of exon 8 of the gene encoding the δ-subunit of the acetylcholine receptor from the patient (patient), his mother (mother), and the two alleles (normal allele, mutant allele) isolated by single-strand conformation polymorphism. Codons 267–270 are indicated by a line and the corresponding single letter amino acid code. The nucleotide affected is indicated by an arrow above each sequence. The sequence of the mutant allele contains a TTT codon (F, phenylalanine), rather than a TCT codon (S, serine) because of a C-to-T substitution in the second position (arrow). The sequence of the patient contains both this position (arrow), indicating the presence of one mutant allele and one wild-type allele in DNA amplified from his δ-subunit exon 8.

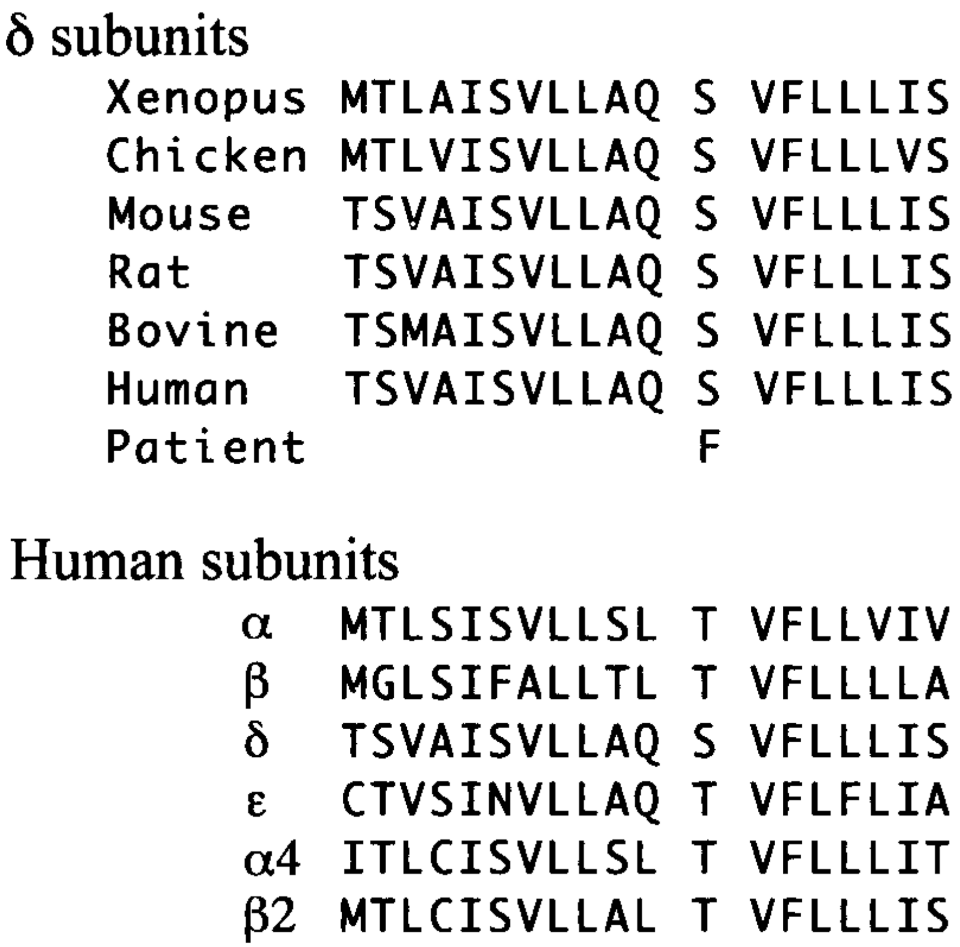

Fig 3.

Alignment of amino acid sequence of M2 domains of normal and mutant δ-subunits and other nicotinic acetylcholine receptor subunits. The residue is 100% conserved among other δ-subunits and highly conserved among other nicotinic receptor subunits.

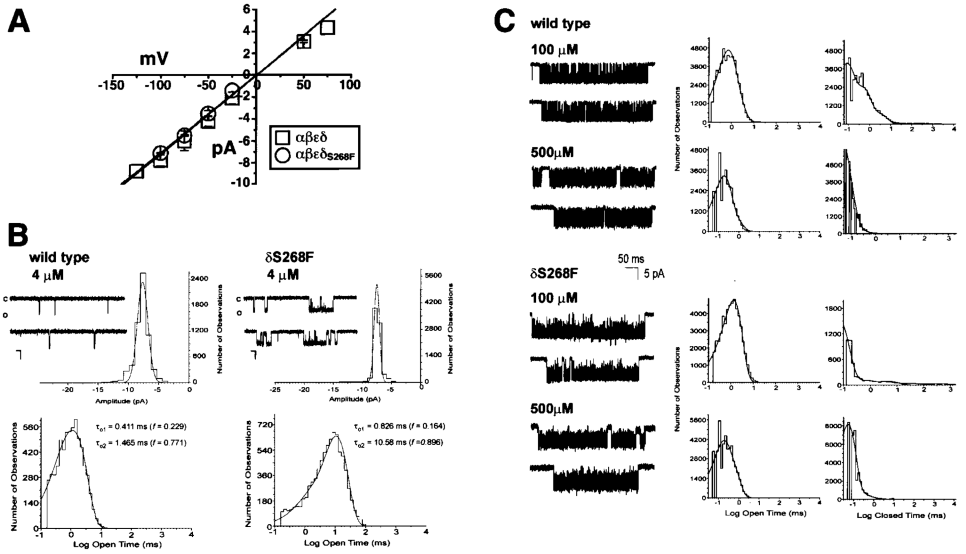

Fig 4.

(A) Current–voltage relationships for single-channel currents recorded from wild-type *(open squares)* or δS268F-acetylcholine receptor (AChR) *(open circles)* expressed in Xenopus oocytes. (B) Wild-type mouse and δS268F AChR single-channel currents recorded at low ACh concentration. AChR single-channel currents recorded from cell-attached patches on Xenopus oocytes expressing wild-type AChR *(left)* and AChRs expressing the δS268F mutation *(right)*. All channels were recorded at a holding potential of −100 mV, 4μm ACh, filtered at 5kHz, sampling rate at 20μsec per point and temperature of 22°C Openings are shown as downward deflections, with close state denoted by the c, and the open state denoted by o. Representative histograms for current amplitude and open time distributions are shown for each of the AChR tested. Amplitude histograms were constructed from events list files created to include all event amplitudes that could be detected. The resulting distribution data was fitted with a Gaussian function with the appropriate number of components. Both the wild-type and mutant AChR show a single amplitude component of − 7.874 ± 0.883 pA and −7.371 ± 0.465 pA, respectively. Open time histograms were fitted with exponential functions of the appropriate number of components using the maximum likelihood algorithm. The wild-type AChR shows two open time constants: τ_{o1} = 0.411 msec (f = 0.229) and τ_{o2} = 1.435 (f = 0.711), while the δS268F AChR shows two open time components of τ_{o1} = 0.826 msec (f = 0.164) and τ_{o2} = 10.582 msec (f = 0.896). Data were filtered at 5kHz for each current sample display. Scale values are 5 pA for the vertical bar and 10 msec for the horizontal bar. The number of patches is included in Table 2. (C) Kinetics of activation of wild-type and δS268F AChR at high ACh concentrations. *(Left)* Single-channel currents elicited by the indicated concentration of ACh recorded from cell-attached patches from Xenopus oocytes expressing adult mouse AChRs containing the wild-type δ *(upper)* or mutated δS268F *(lower)* subunit. Recordings were done at holding potential of −100 mV, filtered at 5kHz, sampling rate at 20μsec per point and temperature of 22°C Channel openings are shown as downward deflections. *(Center* and *right)* Open and closed time duration histograms for adult mouse AChRs containing the wild-type δ *(upper)* or mutated δS268F *(lower)* subunits generated and fitted using pSTAT6. Fitting was done

using the simplex least-squares algorithm. Values of rate constants are shown in Table 3. Single-channel currents displayed were filtered at 4kHz.

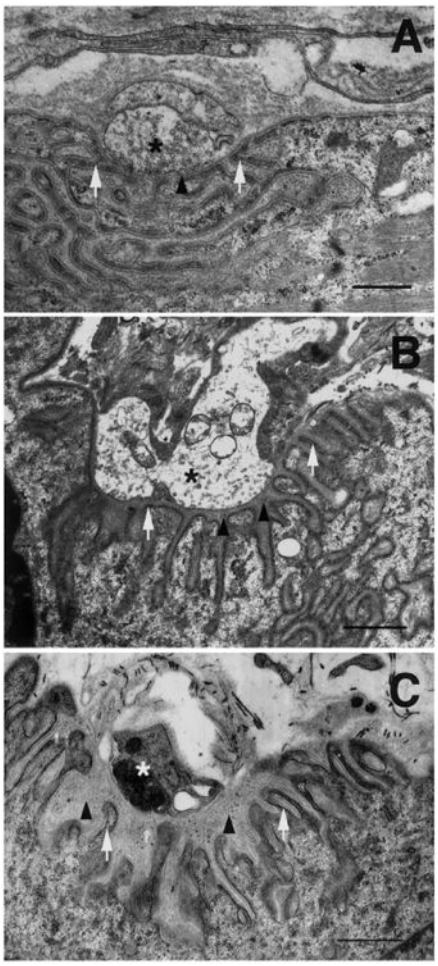

Fig 5.

Electron micrographs of neuromuscular junctions from serial biopsies of patient bearing δS268F mutation. (A) Biopsy 1, intercostal muscle at age 16 months. Nerve terminal *(asterisk)*, synaptic cleft *(black arrowhead)* and endplate folds *(white arrow)* are normal. (B) Biopsy 2, left anconeus muscle at age 9 years. Nerve terminal *(asterisk)* and endplate folds *(white arrow)* are normal. The synaptic cleft is obviously widened and contains dense granular debris *(black arrowhead)*. (C) Biopsy 3, right anconeus muscle at age 15 years. Nerve terminal *(asterisk)* and endplate folds *(white arrow)* are normal. The synaptic cleft is substantially wider than that of biopsy 2 and contains a greater amount of dense granular debris *(black arrowhead)*. Scale bars = 0.33 μm (A); 0.62μm (B); 0.49μm (C).

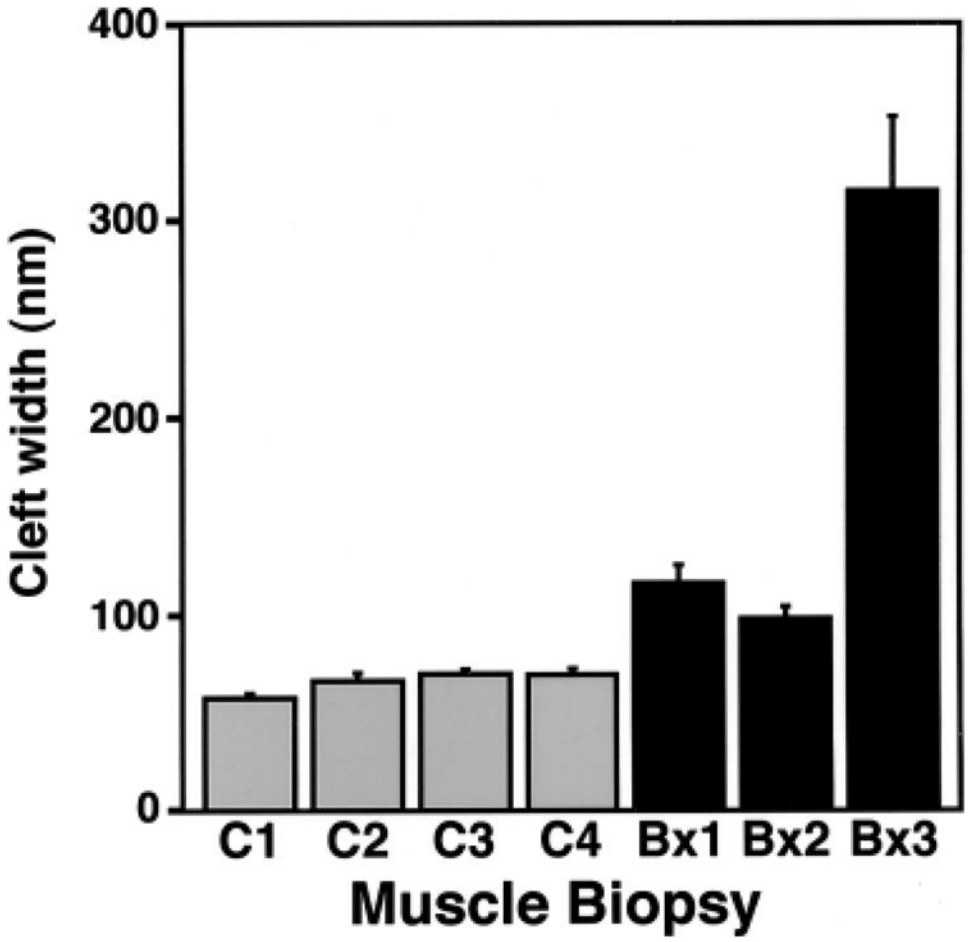

Fig 6.

Synaptic cleft widening in slow-channel congenital myasthenic syndrome. The width of the synaptic cleft for control biopsies *(gray bars)* is relatively uniform for 4 individuals. Cleft width for all three patient biopsies *(black bars)* is more variable and is significantly greater than controls. The cleft width is greatly enlarged at age 15, corresponding to severe progression of weakness. Shown are mean ±SEM for the relative cleft width determined at five to seven sites per neuromuscular junction normalized to the width of the Z lines. A value of 0.1μm for the thickness of the Z lines[20] was used to calculate the absolute cleft widths (nm). Controls (C): 1: 57 ± 6 (n = 12); 2: 66 ± 4 (n = 6); 3: 69 ± 2 (n = 8); 4: 69 ± 3 (n = 10). Patient biopsy (Bx) 1: 115 ± 9 (n = 14, $p < 0.001$, biopsy 1 vs control); patient biopsy 2: 97 ± 6 (n = 6); biopsy 3: 315 ± 37 (n = 8, $p < 0.001$ biopsy 3 vs biopsy 1. 2).

Table 1

Serial Microelectrode Studies of Neuromuscular Transmission in the Slow Channel Congenital Myasthenic Syndrome

Measurement	Control	Biopsy 2	Biopsy 3
MEPP amp. (mV)	0.83 ± 0.04 (n = 82)	0.47 ± 0.10[a] (n = 7)	0.22 ± 0.06[b] (n = 6)
EPP QC (1Hz)	22.61 ± 3.00 (n = 16)	17.93 ± 7.97 (n = 4)	9.64 ± 5.05[c] (n = 10)
MEPC amp (nA)	4.55 ± 0.28 (n = 11)	1.75 ± 0.23[c] (n = 4)	NA
MEPC decay time constant (ms)	3.58 ± 0.16 (n = 11)	23.11 ± 8.25 (n = 4)	NA
EPC amplitude (nA)		15.71 ± 7.97 (n = 12)	8.90 ± 3.75[d] (n = 14)
EPC rise time (ms)		0.33 ± 0.21 (n = 12)	0.94 ± 0.35[b] (n = 14)

[a] $p < .025$ compared with control.

[b] $p < .001$ compared with biopsy 2.

[c] $p < .005$ compared with control.

[d] $p < .05$ compared with biopsy 2.

Table 2

Single-Channel Parameters at Low ACh Concentration

AChR	[ACh] (mM)	Patches/Events[a]	τ_{o1} (msec)	Fraction	τ_{o2} (msec)	Fraction	Rate ($1/\tau o$)	
							$\alpha 1$ (s^{-1})	$\alpha 2$ (s^{-1})
wt	4	3/6886	0.411	0.229	1.465	0.771	2433	683
δS268F	4	6/8906	0.826	0.164	10.58	0.896	1211	95

Single-channel data were recorded in cell-attached patches at a holding potential of −100 mV, 5 kHz and 22°C. The sampling rate was set at 20μsec per point for data acquisition.

[a]No. of patches/No. of events.

Table 3

Single-Channel Parameters at High ACh Concentrations

							Rate ($1/\tau_o$)								Rate ($1/\tau_c$)		
AChR	**[ACh] (mM)**	**Patches/ Burst/Events[a]**	**τ_{o1} (msec)**	**Fraction**	**τ_{o2} (msec)**	**Fraction**	**α1 (s^{-1})**	**α2 (s^{-1})**	**τ_{c1} (msec)**	**Fraction**	**τ_{o2} (msec)**	**Fraction**	**τ_{o3} (msec)**	**Fraction**	**β1 (s^{-1})**	**β2 (s^{-1})**	**β3[b] (s^{-1})**
wt	100	6/143/48191	1.411	0.369	0.583	0.631	709	1715	0.401	0.361	0.063	0.509	2.524	0.129	2494	15873	396
	500	3/87/25474	0.600	0.210	0.169	0.790	1667	5917	0.070	0.246	0.034	0.739	0.297	0.015	14286	29412	3367
δS268F	100	7/188/52349	0.708	0.357	1.744	0.643	1412	573	0.485	0.050	0.064	0.900	4.826	0.050	2062	15625	207
	500	4/102/43209	0.463	0.462	0.137	0.538	2160	7299	0.239	0.056	0.052	0.926	0.861	0.018	4184	19230	1161

Single-channel data were recorded in cell-attached patches at a holding potential of −100 mV, 5 kHz, and 22°C. The sampling rate was set at 20μsec per point for data acquisition.

[a] No. of patches/No. of bursts/No. of events.

[b] Rate constant of the block state.